Temporally Consistent Snow Cover Estimation from Noisy, Irregularly Sampled Measurements

Dominic Rüfenacht[1], Matthew Brown[2], Jan Beutel[3], and Sabine Süsstrunk[1]
[1]*School of Computer and Communication Sciences, EPFL, Switzerland*
[2]*Department of Computer Science, University of Bath, UK*
[3]*Computer Engineering and Networks Lab, ETH Zurich, Switzerland*
{*dominic.ruefenacht, sabine.susstrunk*}*@epfl.ch, m.brown@bath.ac.uk, beutel@tik.ee.ethz.ch*

Keywords: Surface Classification, Gaussian Mixture Models of Color, Markov Random Fields.

Abstract: We propose a method for accurate and temporally consistent surface classification in the presence of noisy, irregularly sampled measurements, and apply it to the estimation of snow coverage over time. The input imagery is extremely challenging, with large variations in lighting and weather distorting the measurements. Initial snow cover estimations are obtained using a Gaussian Mixture Model of color. To achieve a temporally consistent snow cover estimation, we use a Markov Random Field that penalizes rapid fluctuations in the snow state, and show that the penalty term needs to be quite large, resulting in slow reactivity to changes. We thus propose a classifier to separate *good* from *uninformative* images, which allows to use a smaller penalty term. We show that the incorporation of domain knowledge to discard *uninformative* images leads to better reactivity to changes in snow coverage as well as more accurate snow cover estimations.

1 INTRODUCTION

PermaSense is a joint computer science and geoscience project. It aims to develop a distributed *wireless sensor network* (WSN) that can be used in extreme environmental conditions in order to measure permafrost related parameters (Hasler et al., 2008). To supplement physical measurements, such as temperature profiles, pressure, and crack dilatation, a digital camera has been adapted for remote operation in the harsh weather conditions of high-alpine locations (Keller et al., 2009a; Keller et al., 2009b). This allows to "measure" the amount of snow coverage, which is relevant since snow acts as an insulating layer and hence influences permafrost thawing.

As part of this project, we develop a method to compute temporally consistent snow cover maps for images taken with this camera. The challenge is that because the camera is exposed to extreme weather conditions, we get a highly irregular and noisy sampling of the snow coverage. While the camera is programmed to take hourly captures, many of the images are *noisy* or uninformative because of precipitation (snow, rain, fog) on the lens, which can cover up large portions of the scene. The sampling is *highly irregular* because many images are either taken at night or not taken at all because the camera is out of battery.

We use a Gaussian Mixture Model (GMM) of color for initial snow cover estimations, and formulate an energy minimization problem that penalizes fast fluctuations in the snow state to achieve temporally consistent results. The key contributions of this paper are:

- A robust algorithm for snow segmentation in challenging real-world time-lapse data;
- An extension of the Gaussian Mixture Markov Random Field (GMMRF) model to classify between a Gaussian foreground and a mixture-of-Gaussian background class;
- A demo that our Markov Random Field (MRF) prior leads to better inference than baseline filtering (median/averaging), with an overall accuracy of 88% on our ground truth set.

The rest of the paper is organized as follows. Section 2 presents work that is related to our problem. In Section 3, we show how single image snow segmentation has been implemented using GMMs of color. Section 4 highlights the particularities of the image database, and explains how we separate *good* from *uninformative* images. In Section 5, we explain how we include spatio-temporal information in order to achieve temporally consistent snow cover estimations. We show and discuss our results in Section 6, and conclude the work in Section 7.

2 RELATED WORK

Bad weather is not necessarily bad for image understanding. For example, (Nayar and Narasimhan, 1999) show that haze can be helpful to aid depth perception. In our case, however, the harsh weather conditions not only change the appearance of the scene, but alter the imaging system (e.g., precipitation on lens, no power to take pictures, etc).

There is previous research that aims to extract information from time-lapse videos of outdoor scenes with varying illumination and weather conditions. (Jacobs et al., 2007) show that the second order statistics of a large database of webcam images can be used to characterise surface orientation, weather, and seasonal change. (Breitenstein et al., 2009) use time-lapse data captured by static webcams with low or varying framerate for unusual scene detection. By defining anything that has been observed in the past as "usual", they are able to detect changes in illumination and weather conditions. In contrast to our dataset, both methods work with imagery that is not distorted by precipitation on the lens, and thus less noisy. Also, none of these datasets is as irregularly sampled as ours.

The problem of creating spatio-temporally consistent scene labellings or classifications from noisy estimates has arisen in various other domains of video processing. In (Khoshabeh et al., 2011), a stereo video disparity estimation method is proposed where initial disparity estimates are treated as a space-time volume. In order to reduce computational complexity, the authors handle spatial and temporal consistency separately, by setting up a l_1-normed minimization with a total variation regularization problem. (Floros and Leibe, 2012) propose a Conditional Random Field (CRF) formulation for the semantic scene labelling problem which is able to achieve temporal consistency. They use 3D scene reconstruction in order to temporally couple individual image segmentations. Both (Khoshabeh et al., 2011) and (Floros and Leibe, 2012) use controlled imaging conditions, without large changes in illumination, weather, and external factors such as precipitation on the lens. Compared to these methods, our approach needs an increased level of robustness.

(Blake et al., 2004) present an interactive background/foreground image segmentation method using a *Gaussian Mixture Markov Random Field* (GMMRF). They propose a novel pseudo-likelihood algorithm that jointly learns the Gaussian color mixtures and the coherence parameters separately for foreground and background. Our work can be seen as an extension of the GMMRF. Instead of inferring the labels of a single mixture, we formulate a 2-class problem with a single Gaussian over one class, and a Gaussian mixture over the other.

3 SINGLE IMAGE SEGMENTATION

Due to various reasons (e.g., varying illumination, wrong white balancing, cast shadows), segmenting snow is not as easy as it may seem. A more sophisticated approach than simple thresholding is needed to get a proper snow segmentation. We use a GMM of color to compute the probability of a pixel belonging to a specific class (snow or not snow), rather than a hard assignment such as one would obtain by using k-means (MacQueen, 1967). Unless otherwise mentioned, we denote the observed value or observation, i.e. the intensity value of a pixel, by the variable z. The binary variable x represents the snow state, where $x = 1$ stands for *snow* and $x = 0$ for *not snow*. We define the following likelihoods:

$$p(z|x=1) = \mathcal{N}(z;\mu_s,\Sigma_s)^1 \tag{1}$$

$$p(z|x=0) = \sum_c p_c \cdot \mathcal{N}(z;\mu_c,\Sigma_c). \tag{2}$$

Equation (1) is a single Gaussian representing the likelihood of *snow*, and Equation (2) is a mixture of c Gaussians accounting for the likelihood of *not snow*. The probability of an observation z can be expressed as:

$$\begin{aligned} p(z) &= \int p(z|x)p(x)dx = \sum_{i=0}^{1} p(z|x=i)p(x=i) \\ &= p_s \cdot \mathcal{N}(z;\mu_s,\Sigma_s) + \sum_c p_c \cdot \mathcal{N}(z;\mu_c,\Sigma_c), \end{aligned} \tag{3}$$

where p_s is the prior of *snow*, and $\sum_c p_c = 1 - p_s$ is the prior of *not snow*. By defining $p_s + \sum_c p_c = \sum_{c'} p_{c'} = 1$, Equation (3) can be written as:

$$p(z) = \sum_{c'} p_{c'} \cdot \mathcal{N}(z;\mu_{c'},\Sigma_{c'}), \tag{4}$$

which is a mixture of $|c'| = |c| + 1$ Gaussians. We fit a mixture of Gaussians to z, and then infer μ_s and Σ_s from the maximum luminance component. Using Bayes formula, we can infer the probability of *snow* given the data we observe:

$$p(x=1|z) = \frac{p(z|x=1)\cdot p_s}{p(z|x=1)\cdot p_s + p(z|x=0)}. \tag{5}$$

[1] $\mathcal{N}(x;\mu,\Sigma) = \frac{1}{(2\pi)^{\frac{n}{2}}(|\Sigma|)^{\frac{1}{2}}} \exp(-\frac{1}{2}(x-\mu)^T\Sigma^{-1}(x-\mu))$

The Bayes classifier we use is, after simplification:

$$x = \begin{cases} 1 & p(x=1|z) > 0.5 \\ 0 & \text{otherwise} \end{cases}. \quad (6)$$

4 THE IMAGE DATABASE

The PermaSense image database we used contains captures of the Matterhorn that were taken between November 2009 and June 2010 (Keller et al., 2009a; Keller et al., 2009b). Figure 1 shows typical images present in the database. Ideally, the camera should

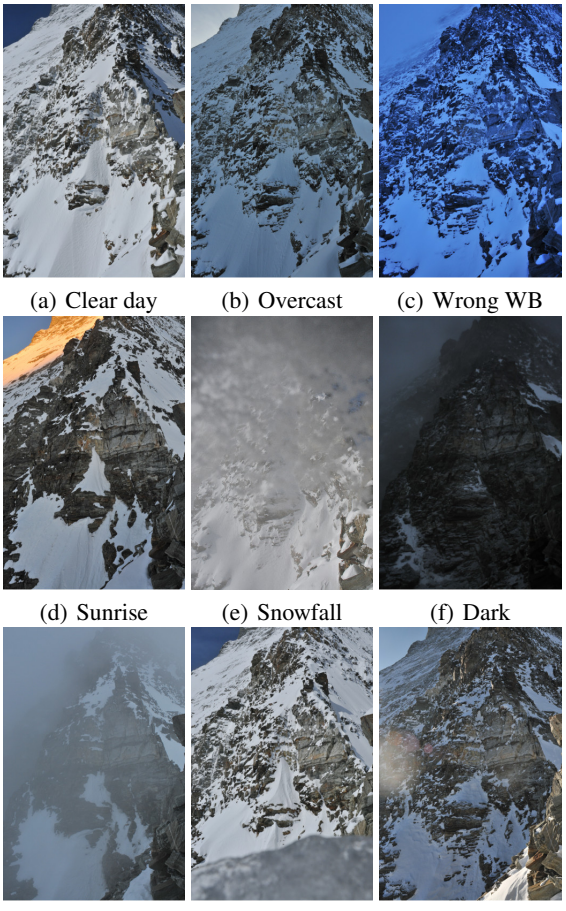

(a) Clear day (b) Overcast (c) Wrong WB

(d) Sunrise (e) Snowfall (f) Dark

(g) Fog (h) Ice on lens (i) Lens flare

Figure 1: Images representing the variety of the image database. All are in our manually labelled ground truth set.

take hourly captures, but since it is powered using solar panels and there are long periods without sunshine, at times the camera cannot operate. In fact, only around 2500 images are present in the database, which is about 50% of the images that should have been taken on an hourly basis. Figure 2 shows the average number of images per week. One can see the

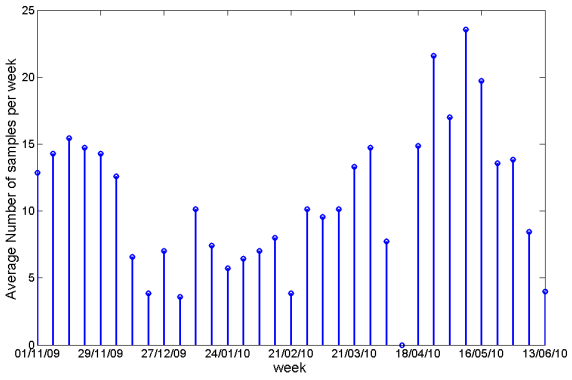

Figure 2: Average number of samples per week.

big variations in the number of images taken. There are even weeks where there is no image taken at all, such as in the first week of April 2010.

4.1 Splitting up the Data

In the following, we denote $L(m,n)$ the intensity value of pixel (m,n) of an image L.[2] Images that are too dark, such as the one in Figure 1(f), are not suited for the GMM of color. We exclude all images whose mean intensity value $\overline{L}$ is below 0.2, i.e. $\overline{L} < 0.2$, and refer to this reduced dataset as *daytime* images.
Using domain knowledge, we are able to identify types of images in the dataset that systematically give wrong snow cover estimations. Our classifier used to select the *good* (informative) images from all *daylight* images is based on the following two observations:

- **Blurry Images:** Snow cover maps we obtain for images that are blurry (i.e., because of fog, see Figure 1(g)) are most often wrong. We apply a Gaussian low-pass filter on L to get L_{low}. The high-frequency components of L are then simply $L_{\text{high}} = L - L_{\text{low}}$. We define a *sharpness index* s by the following ratio:

$$s = \frac{\sum_m \sum_n |L_{\text{high}}(m,n)|^2}{\sum_m \sum_n |L_{\text{low}}(m,n)|^2}. \quad (7)$$

  Since we want to drive our model using *good images*, it is less acceptable to have false-positives than false-negatives. We manually tagged 250 *good* and 250 *uninformative* images, and then set the threshold on s such that we have a false-positive rate of less than 1%. Figure 3 shows the histogram for the sharpness index computed for the selected 250 *good* and 250 *uninformative* images. The green vertical line at $s = 0.0289$ indi-

[2] $z = L(m,n)$

cates where the above condition was satisfied. We therefore exclude all images where $s < 0.0289$.

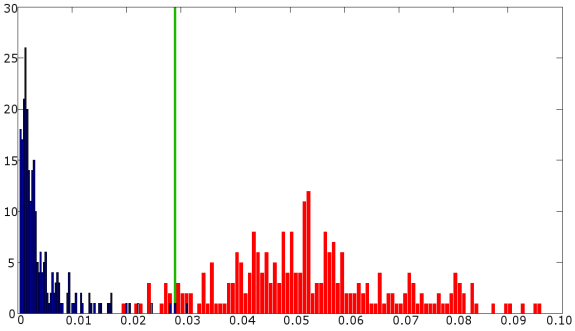

Figure 3: Histogram of the sharpness indexes computed for the 250 *good* (red) and the 250 *uninformative* (blue) images. The green vertical line shows the smallest value of the sharpness index such that there are less than 1% false-positives.

- **Sunny Images:** In images taken on a sunny day, the rock in the middle casts a big shadow onto the snow, as can be seen in Figure 1(a). This results in the fact that the shadowed pixels are no longer detected as snow. We found that these images can be quite well excluded by imposing a threshold on the minimum of the negative snow likelihoods:

$$\min_i -\log p(z_i|x_i = 1) < T_1. \qquad (8)$$

  In our case, $T_1 = -5$ allowed to best discriminate between *good* and *uninformative* images.

After discarding the images labelled as uninformative (728 dark, 766 blurry, 358 sunny images), we are left with 659 *good* images. Note that 2396 of the 2491 images present in the image database were classified correctly, giving an overall classification correctness of **96.2%**. The false-positive rate on all images is **1.8%**. It is worth noting that "foggy" and "sunny" images could give more information about the scene (e.g., cues for 3D structure), but this is left for future work.

5 TEMPORAL CONSISTENCY

We achieve temporal consistency by formulating an energy minimization problem, which involves the initial snow cover estimates computed in Section 3 as well as a penalty term for different assignments. We also tested weighted average and median filtering for comparison.

5.1 Markov Random Fields (MRF)

Traditional filtering approaches such as (weighted) average and median filtering are not sensitive to the data, they simply smooth it. We therefore used an MRF, which have a data term and a prior term. In its general form, an MRF can be written as follows:

$$p(z,x) = \prod_i p(z_i|x_i) \cdot \prod_i \prod_{j \in N(i)} p(x_i,x_j), \qquad (9)$$

where i indexes over all pixels in space and time, and $N(i)$ is the set of neighbors directly adjacent to pixel i in space and time dimensions. Taking the log, the products "simplify" to sums, and we get the following global energy function we want to minimize:

$$-\log p(z,x) = \sum_i f_1(z_i,x_i) + \sum_i \sum_{j \in N(i)} f_2(x_i,x_j), \qquad (10)$$

where the data term $f_1(z_i,x_i) = -\log p(z_i|x_i)$ is the negative log likelihood, computed using the GMM of color (see Section 3). For the prior term, we use a Potts Model $f_2(x_i,x_j) = \lambda_{i,j}|x_i - x_j|$, which can be seen as a penalty for a change in snow-state in space or time dimensions. The minimum of the global energy function in Equation (10) can be efficiently computed using Graph Cuts (Boykov et al., 2001). With $\lambda_{i,j}$ we set how strong the bond between two neighboring pixels i and j is, which controls the amount of smoothing in the spatial domain and the number of snow changes in the temporal domain.
Ideally, one would stack up all the informative images present in the database and apply Graph Cuts on the whole block to find the best solution. With the aim of reducing the memory requirements, we applied Graph Cuts separately in the spatial and the temporal domain by only connecting adjacent pixel neighbors in space and time, respectively. We observed that in order to get temporally smooth results, it is sufficient to connect each pixel with its neighbors in time, and to apply Graph Cuts on those *time vectors* independently. We denote the resulting image at time instant t with penalty term λ as H^t_λ. For comparison, we implemented two traditional filtering approaches.

5.2 Weighted Average Filtering

The Gaussian filtered snow cover map at time instant t $G^t_{r_1,r_2}$ is computed as follows:

$$G^t_{r_1,r_2}(m,n) = \sum_{k=-r_2}^{r_2} \sum_{i=-r_1}^{r_1} \sum_{j=-r_1}^{r_1} w_{i,j,k} \cdot L^{t+k}(m+i,n+j), \qquad (11)$$

$$w_{i,j,k} = \frac{1}{2\pi\sigma_1^2} \frac{1}{\sqrt{2\pi\sigma_2{}^2}} e^{-\frac{1}{2}\left(\frac{i^2+j^2}{\sigma_1^2} + \frac{k^2}{\sigma_2^2}\right)}, \qquad (12)$$

where $r_1, r_2 \in \mathbb{Z}$ define the spatial and temporal filter size, and σ_1 and σ_2 are chosen such that the Gaussian weights approach zero for $i = j = \pm r_1$ and $k = \pm r_2$, respectively.

5.3 Median Filter

The median filter is known to be robust to outliers. The median filtered snow cover estimation map $M^t_{r_1,r_2}$ is computed as follows:

$$M^t_{r_1,r_2}(m,n) = \text{med}\{L^{t-r_2}(m-r_1,n-r_1),\ldots, L^{t+r_2}(m+r_1,n+r_1)\}, \quad (13)$$

where med$\{\cdot\}$ denotes the median operator.

6 RESULTS AND DISCUSSION

6.1 Ground Truth

We created binary ground truth of 19 images by hand-labelling pixels using GIMP (see Figure 4). They

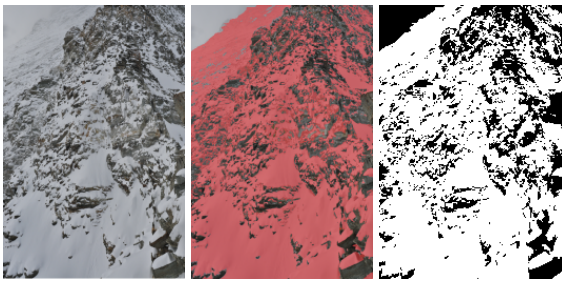

(a) Input image (b) Snow pixels labelled in GIMP (c) Binary ground truth map

Figure 4: How the binary maps were created. We created a new layer in GIMP, where all snow pixels of the input image (a) were painted in red (b). Every red pixel was then assigned a "1", and the rest a "0", which results in the binary snow map shown in (c).

represent the variability of the image dataset, sampled over the whole time span of the set. Examples of images in the ground truth set are shown in Figure 1, as well as Figure 9. For images where parts are obstructed, such as Figure 1(e), we used information from the nearest unobstructed neighbors in time to get as close as possible to the true amount of snow coverage. We compare the ground truth on a pixel-by-pixel basis with the resulting snow cover maps of the different methods. As we exclude certain images, it can happen that we do not have an estimate at the time instant of the ground truth image (e.g., only 7 out of the 19 ground truth images were labelled as *good* images). In order to compute the classification correctness, we thus took the snow cover map closest in time (see Figure 5).

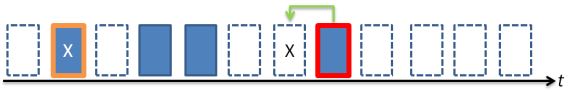

Figure 5: Dashed rectangles represent all images in the database, "X" marks a ground truth image, filled rectangles are computed snow cover estimates. Maps are compared pixel-wise (orange rectangle). If the estimate for a ground truth does not exist, we select the one closest in time (red rectangle).

6.2 Finding the Best Parameters for GMM of Color

Being a parametric model, the GMM has several parameters one can optimize. We tested several combinations of number of mixture components, as well as type of covariance matrix Σ (spherical and full). We also transformed the images to the most relevant color spaces before applying the GMM of color. We found that the results were generally better using a spherical covariance matrix. Figure 6 shows the accuracy obtained for different combinations of number of mixture components and color spaces using a spherical covariance matrix.

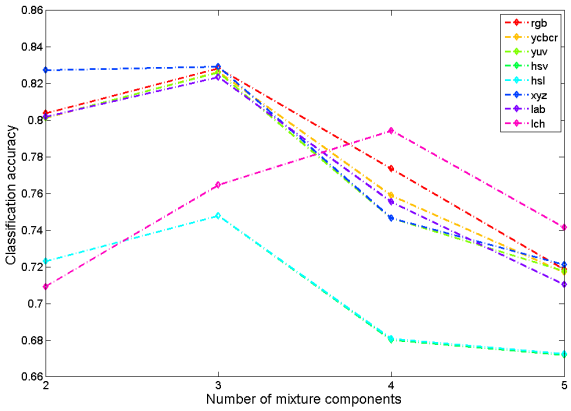

Figure 6: Results for different color spaces and number of mixture components, using a spherical covariance matrix.

We can see that with the exception of the Lch color space, best results are always obtained for three mixture components. When it comes to selecting the color space, we can see that XYZ slightly outperforms the standard sRGB color space, as well as the opponent color spaces we tested. The accuracy for HSV and HSL is almost 10% lower than for the other color spaces, so these two are not well suited for snow segmentation.

6.3 Filtering Parameters

Our goal is to obtain an accurate, temporally consistent estimation of snow coverage. There are different reasons why snow cover estimations based on single images are inaccurate. As mentioned in Section 4, quite a lot of the images are corrupted by external factors, which influence the quality of our snow classification using a GMM of color: Shadows cast on snow results in the fact that these regions are wrongly classified as "not snow", reflections of the sunlight on (wet) stone makes those regions very bright, and hence they are misclassified as "snow" (see Figure 9(d)). Even more problematic is precipitation on the lens, as well as foggy weather, which leads to large parts of the image that are misclassified. To a smaller extent, there might also be misclassification due to sensor noise. We investigated various combinations of spatial and temporal filter lengths for both the weighted average and the median filter, as well as different weights for the MRF.

Median Filter Since the median filter generally gave better results than the weighted average approach, we show the accuracy obtained for various combinations of spatial and temporal filter sizes for the median filter (see Figure 7). Note that the temporal half filter length r_1 was increased by factors of 2.

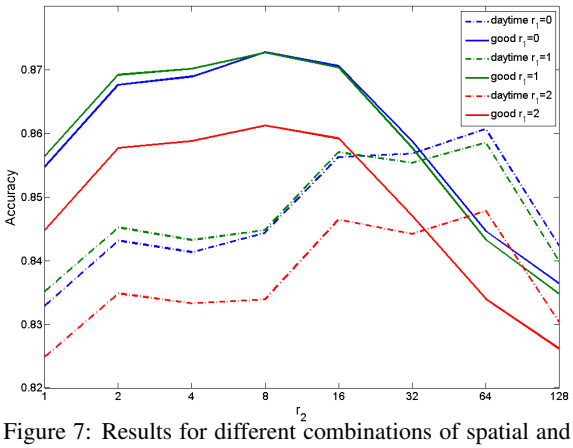

Figure 7: Results for different combinations of spatial and temporal filter sizes using median filter, for both the *daytime* and the *good* image set.

The best results are obtained using only the *good* images. We can see that the filter size can be reduced by a factor of 8 as compared to the *daytime* images (from 64 to 8), since there are fewer wrong snow estimates. This allows the filter to faster adapt to changes. We also see that the results drop by more than 1% for a spatial filter size $r_2 = 2$ as compared to smaller filter sizes. We found that $r_2 = 1$ resulted in slightly more temporal consistent results, which is why we set $r_2 = 1$.

MRF As mentioned before, the MRF was only applied in the temporal domain because of computational complexity and memory requirements. Figure 8 shows the results for various weights λ:

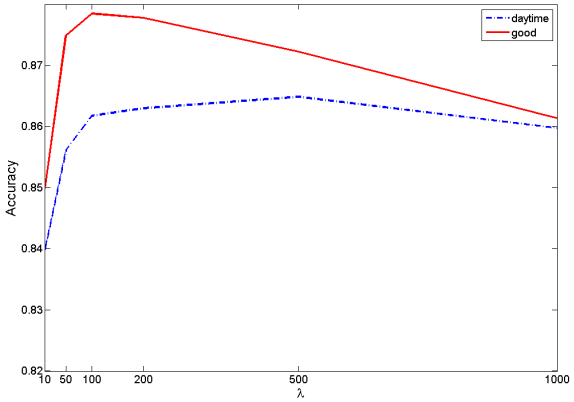

Figure 8: Results for different weights using for the MRF, for both the *daytime* and the *good* image set.

As with the median filter, the results are consistently better when using only the *good* images. The weight λ can be set lower, which results in better reactivity to changes in snow coverage. This justifies the exclusion of uninformative images.

6.4 Comparison of the Methods

Table 1 summarizes the best results obtained for each method on our ground truth set, both for all *daytime* images, as well as for the *good* images only. The reactivity to changes in snow coverage as well as the temporal smoothness were subjectively evaluated by watching a time lapse video. The videos can be found on our web page[3]. One can see the trend that the results are better for the *good* images, irrespective of the

Table 1: Overall classification correctness (C), standard deviation (σ), and reactivity to changes in snow coverage (R) on 19 images, for the Gaussian Mixture Model (GMM), weighted average (WA), median (Med), and Markov Random Field (MRF), using the *daytime* or the *good*† images.

Method	C	σ	R
GMM of color	83.3	8.7	immediate
WA	85.6	7.3	slow
Med	86.1	6.9	slow
MRF	86.5	6.6	fast
WA†	86.5	7.6	slow
Med†	87.2	6.8	fast
MRF†	**87.9**	**6.1**	**very fast**

[3] http://ivrg.epfl.ch/research/snow_segmentation/

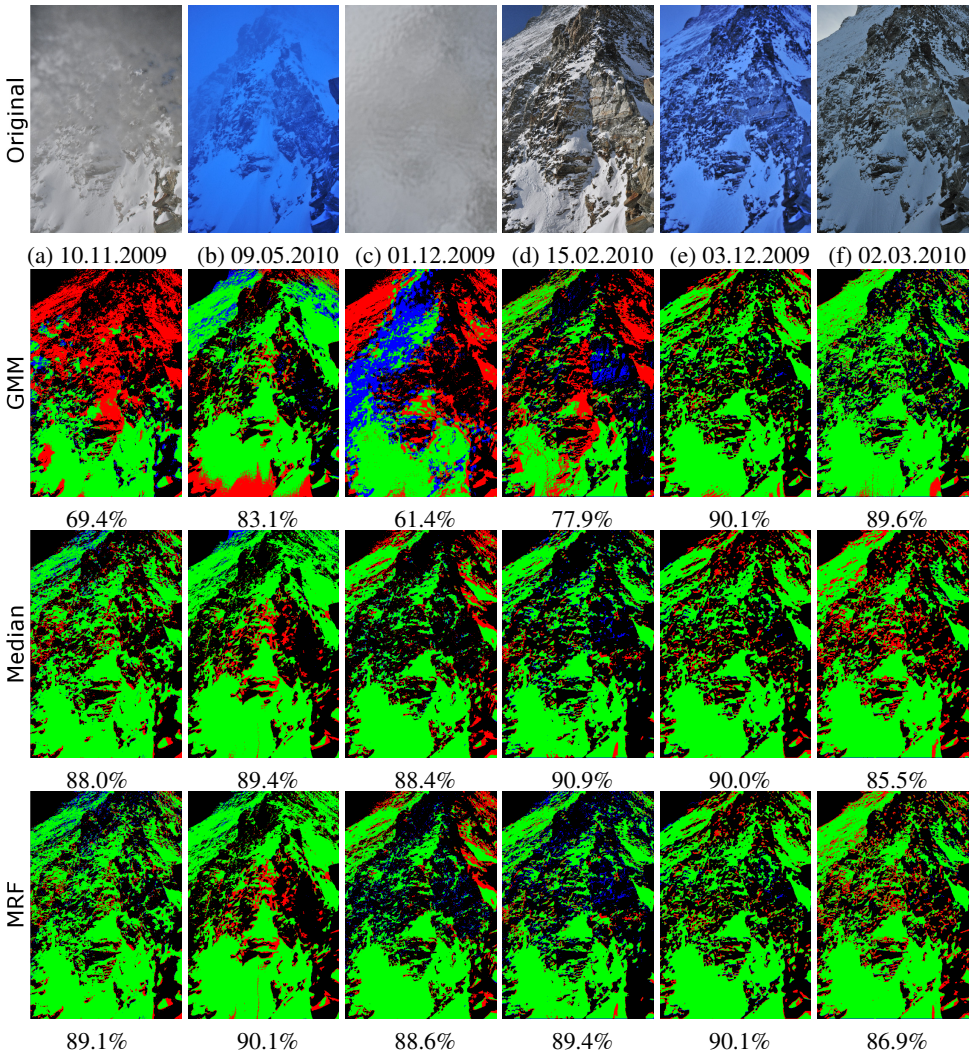

Figure 9: Comparison of the methods. Green are the true positives, blue the false positives, red the false negatives, and black the true negatives. First row are the originals, second row the results of the GMM of color. Rows three and four show the results obtained for the median filtering approach $M^t_{1,8}$ and the MRF H^t_{100}, respectively.

method used to achieve temporal consistency. Figure 9 shows results obtained on the *good* images. Images (a)–(c) are examples where the temporal information can significantly improve the classification accuracy, because the images are distorted. Image (d) is interesting because it shows how the GMM of color is fooled by shadows (upper right side), as well as illuminated rock (center right part), which are both misclassified. Again, one can see how the results improve by incorporating information from neighboring images in time. Images (e) and (f) both give reasonable results using the GMM of color. In fact, using temporal information slightly deteriorates the accuracy of the snow maps, because the snow coverage is different in neighboring images. The MRF gives slightly better results than the median filter approach, because it is able to faster adapt.

Not only the classification correctness is the highest for the MRF approach, but this method is also temporally smooth and reacts very fast to changes in snow coverage. This is due to the fact that the MRF is not just a simple smoothing of the labels, as in the median filter, but in fact a data-sensitive and temporally smooth labelling. This is a big advantage of the MRF over the two basic filtering approaches, as is exemplified in Figure 10, where two consecutive images of the database are shown. The image at instant t (2. February 2010, 11.30am) is the last one taken just before the one at $t+1$ (3. February 2010, 2.26pm). A major snow fall happened in-between, which explains the important changes in snow coverage. Note how the median filter approach is unable to adapt to the

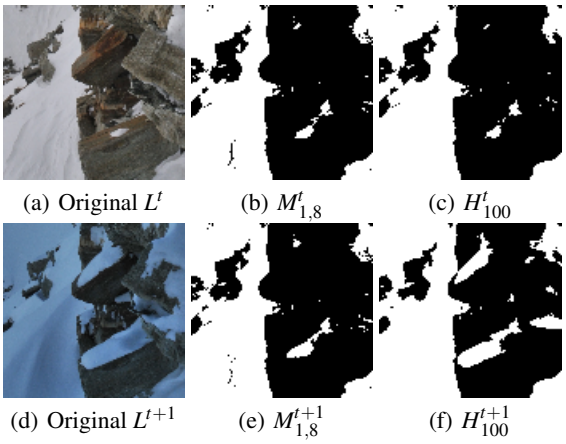

(a) Original L^t (b) $M^t_{1,8}$ (c) H^t_{100}

(d) Original L^{t+1} (e) $M^{t+1}_{1,8}$ (f) H^{t+1}_{100}

Figure 10: Crop of two consecutive snow maps, before and after a major snow fall. (a) and (d) are the originals, (b) and (e) the median filtered maps M^t, and (c) and (f) the MRF H^{t+1}. The MRF almost completely reacts to the change in snow coverage.

changes and underestimates the amount of snow coverage at time instant $t+1$, whereas the MRF approach is adapting almost completely.

7 CONCLUSIONS AND FUTURE WORK

We propose a technique for robust snow cover estimation from time-lapse imagery. Since many of the images are uninformative, single image snow segmentation using GMM of color is insufficient to get temporally consistent results. We use Markov Random Fields (MRF) and formulate the temporal consistency problem as an energy minimization, where we use a penalty term to penalize neighboring pixels (spatially and temporally) with different labels. Due to the nature of the image data, the weight of the penalty term has to be quite large in order to provide temporally consistent results. The higher the weight, the less reactive the model is to changes in snow coverage. Using domain-knowledge, we propose a classifier to exclude most of the *uninformative* images. Using only the *good* images allows to relax the temporal constraints, making the model more reactive to changes. The proposed model is both robust to outliers as well as very reactive to changes in snow coverage.

Future work includes attempting the joint optimization over space and time of Equation (10), and the implementation of a snow deposition model, which would be useful for long periods of *uninformative* and/or missing images. This model could be used instead of the zero-order hold we applied, resulting in smoother transitions between two *good* images. Another interesting path to follow is to have different models for different weather states, which could help improve the initial snow cover estimations.

ACKNOWLEDGEMENTS

This work is in part supported by the National Competence Center in Research on Mobile Information and Communication Systems (NCCR-MICS), a center supported by the Swiss National Science Foundation under grant number 5005-67322.

REFERENCES

Blake, A., Rother, C., Brown, M., Perez, P., and Torr, P. (2004). Interactive image segmentation using an adaptive GMMRF model. *European Conference on Computer Vision (ECCV)*, pages 428–441.

Boykov, Y., Veksler, O., and Zabih, R. (2001). Fast approximate energy minimization via graph cuts. *IEEE Transactions on Pattern Analysis and Machine Intelligence*, 23(11):1222–1239.

Breitenstein, M. D., Grabner, H., and Van Gool, L. (2009). Hunting Nessie - Real-Time Abnormality Detection from Webcams. *IEEE International Conference on Computer Vision (ICCV)*, pages 1243–1250.

Floros, G. and Leibe, B. (2012). Joint 2D-3D temporally consistent semantic segmentation of street scenes. *IEEE Conference on Computer Vision and Pattern Recognition (CVPR)*.

Hasler, A., Talzi, I., Beutel, J., Tschudin, C., and Gruber, S. (2008). Wireless sensor networks in permafrost research-concept, requirements, implementation and challenges. *Proceedings of the 9th International Conference on Permafrost (NICOP)*.

Jacobs, N., Roman, N., and Pless, R. (2007). Consistent temporal variations in many outdoor scenes. *IEEE Conference on Computer Vision and Pattern Recognition (CVPR)*.

Keller, M., Beutel, J., and Thiele, L. (2009a). Demo Abstract: MountainviewPrecision Image Sensing on High-Alpine Locations. *Adjunct Proceedings of the 6th European Workshop on Sensor Networks (EWSN)*, pages 15–16.

Keller, M., Yücel, M., and Beutel, J. (2009b). High-Resolution Imaging for Environmental Monitoring Applications. *Proc. International Snow Science Workshop*, pages 197–201.

Khoshabeh, R., Chan, S. H., and Nguyen, T. Q. (2011). Spatio-temporal consistency in video disparity estimation. In *IEEE International Conference on Acoustics, Speech and Signal Processing (ICASSP)*, pages 885–888.

MacQueen, J. (1967). Some methods for classification and analysis of multivariate observations. *Proceedings of the fifth Berkeley symposium on Mathematical Statistics and Probability*, pages 281–297.

Nayar, S. and Narasimhan, S. (1999). Vision in bad weather. *IEEE International Conference on Computer Vision (ICCV)*, pages 820–827.